Inorganic Chemistry

Article

Cite This: *Inorg. Chem.* 2020, 59, 1556−1565

pubs.acs.org/IC

Where Is the Fluoro Wall?: A Quantum Chemical Investigation

Julian D. Rolfes, Maurice van Gastel,* and Frank Neese*

Max-Planck-Institut für Kohlenforschung, Kaiser-Wilhelm-Platz 1, D-45470 Mülheim an der Ruhr, Germany

Supporting Information

ABSTRACT: Despite their isoelectronic properties, fluoro and oxo ligands exhibit completely different chemical behavior. Formally speaking, the first is known to exclusively form single bonds, while the latter is generally observed to form double (or even triple) bonds. The biggest difference, however, lies in what is known among inorganic chemists as the Oxo Wall: the fact that six-coordinate tetragonal transition metal oxo complexes are not observed beyond group 7 elements. While the Oxo Wall was explained a few decades ago, some questions regarding the nature of the Oxo Wall remain unanswered. For example, why do group 8 oxo complexes with high oxidation states not violate the Oxo Wall? Moreover, why are transition metal fluoro complexes observed through the whole transition metal series? In order to understand how the small difference between these two isoelectronic ligands can give rise to such different chemical behaviors, we conducted an extensive computational analysis of the geometric and electronic properties of model fluoro and oxo complexes with metals around the Oxo Wall. Among many insights into the details of the Oxo Wall, we mostly learned that the oxygen 2p orbitals are prone to meaningfully interact with transition metal d orbitals, because they match not only spatially but also energetically, while for fluorine the p orbital energies are lower to an extent that interaction with transition metal d orbitals is much reduced. This in turn implies that in those instances where the metal d orbitals principally accessible for interaction are occupied, the oxygen 2p orbitals are too exposed to be stable.

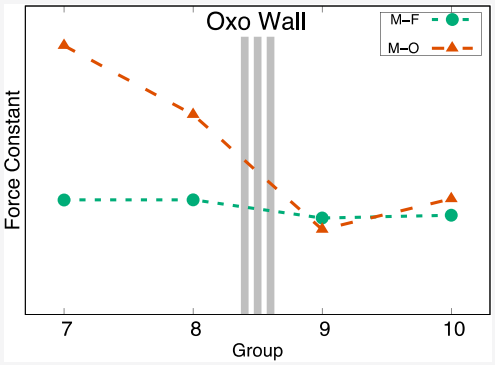

INTRODUCTION

The Oxo Wall is a widely known and accepted concept among the inorganic chemical community.[1] It states the instability of six-coordinate tetragonal oxo complexes with metals beyond group 8 (Figure 1).

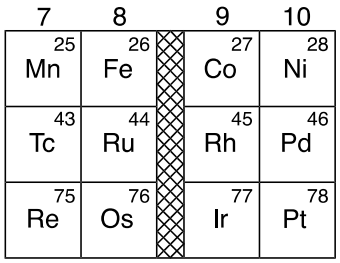

Figure 1. Depiction of the Oxo Wall surrounded by the investigated transition metals.

While transition metal oxo complexes are a prominent motif in biological oxidation processes,[2,3] the concept of the Oxo Wall dates back to 1962 when Ballhausen and Gray developed a molecular orbital energy level scheme that correctly described the electronic structure of the vanadyl ion.[4] The description of chromyl and molybdenyl ions followed shortly after, where the metal−oxo interaction was represented as a triple bond for the first time.[5] This notion is based on elementary molecular orbital considerations in which the bond order is deduced by subtracting the number of electrons in antibonding orbitals of a given bond from the number of electrons in the bonding counterparts of these orbitals and dividing the result by two.[6] For example, in the six-coordinate tetragonal oxo complex $Mo(V)OCl_5^{2-}$ the single d electron is found in the nonbonding d_{xy} orbital, leaving the two other d orbitals of t_{2g} symmetry (d_{xz} and d_{yz}) amenable to π interactions with the $p_{x/y}$ orbitals from the oxo ligand on the z axis (Figure 2). A total of six electrons are present in the two bonding π-orbitals and the bonding σ-orbital (interaction between oxo p_z and metal d_{z^2} orbital), while all antibonding counterparts are empty, thus leaving a metal−oxo triple bond.

The theoretical concept of the Oxo Wall—as stated by Gray and Winkler is as follows: "Complexes with tetragonal symmetry can have no more than 5 d electrons and still retain some MO multiple bonding. In the absence of π-bonding to the metal, the oxo will be extremely basic and unstable with respect to protonation or attack by electrophiles."[1] This is also supported by a large array of experimental investigations.[7−9] While oxo compounds are known with transition metals beyond the Oxo Wall[10,11] with well-characterized electronic structure,[12] these do not violate the concept of the Oxo Wall because they are not of tetragonal symmetry. Claims that exceptions have been found[13] were later retracted and as such, "the 'Oxo Wall' stands."[14]

Received: November 27, 2019
Published: January 7, 2020

DOI: 10.1021/acs.inorgchem.9b03474
Inorg. Chem. 2020, 59, 1556−1565

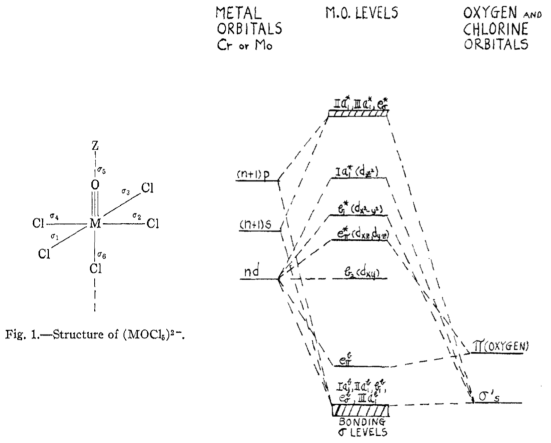

Fig. 1.—Structure of $(MOCl_4)^{2-}$.

Fig. 2.—Relative energies of the one-electron molecular orbitals for the $(MOCl_4)^{2-}$ molecule ion.

Figure 2. Original figures of Gray and Hare[5] that provided the historic foundation for the concept of the Oxo Wall. The figure depicts a metal oxo triple bond for the first time (left), reasoned by MO considerations (right). Reprinted from ref 5. Copyright 1962 American Chemical Society.

Extrapolation of this concept to the immediate neighbors of oxygen in the periodic table appear to be logical and seem to imply the existence of a Nitrido Wall as well as a Fluoro Wall. Interestingly, so far, nitrido complexes beyond the Nitrido Wall (which has the same location as the Oxo Wall) are not known, and even imido complexes are scarce.[15,16] In contrast, late transition metal fluoro complexes are widely observed and scrutinized.[17−19] Hence, the question arises, why do the considerations for the Oxo Wall not hold for the isoelectronic fluoro ligand? In order to answer this question, we investigate and compare the electronic properties of several *in silico* transition metal fluoro and oxo complexes around the Oxo Wall with the goal of understanding the differences between the fluoro and oxo ligands as well as to gain deeper insight into the electronic origin of the Oxo Wall.

In doing so, we took a strictly conceptual approach in which we studied *in silico* yet realistic models of transition metal oxo and fluoro complexes around the Oxo Wall (Figure 3). The

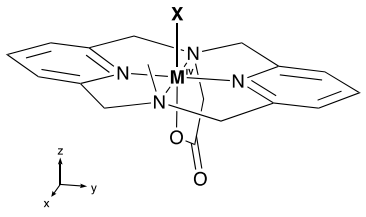

Figure 3. Schematic structure of the used model complex with indication of the coordinate system. The considered transition metals are given in Figure 1; X = F^- or O^{2-}.

study sheds light on the changes in the nature of the metal oxo and metal fluoro bonds, as well as in the electronic structure of the d manifold by employing density functional theory (DFT) as well as complete active space self-consistent field (CASSCF) followed by second-order N-electron valence perturbation theory (NEVPT2). We evaluate electronic properties, force constants, orbital splittings (*via ab initio* ligand field theory, AILFT),[20,21] and NMR shift parameters. Some of these properties are, in principle, amenable to experimental studies, while others serve illustrative and interpretative purposes.

METHODS

All computations were performed with the ORCA program package.[22,23] DFT calculations were performed with the PBE0 functional[24] and the def2-TZVP basis set[25] including Grimme's D3 dispersion correction with the Becke−Johnson damping scheme.[26,27] The resolution of identity approximation[28] was used for the Coulomb integrals with the def2/J auxiliary basis set[29] and for the Hartree−Fock exchange terms with the chain of spheres (COSX) approximation.[30] Unless otherwise noted, all geometries were built from scratch using the molecular builder in the Avogadro[31] program and subsequently optimized by DFT. Local minima were confirmed through frequency analysis. Self-consistent field (SCF) and optimization convergence criteria were set tightly (ORCA keywords "TightSCF" and "TightOpt"). These settings were used for the spin state and orbital analysis as well as the generation of all parameters given below except the AILFT and AOM parameters. Orbital analysis was carried out on the set of quasi-restricted orbitals (QRO)[32] (ORCA keyword "UNO").

For AILFT and AOM parameters, state-averaged complete active space self-consistent field (CASSCF)[33−35] calculations were performed on an active space of the five metal d-based orbitals (CAS(X,5)) with the def2-TZVP basis set and the AILFT module.[20,21] Tight SCF convergence criteria including the TrafoStep RI approximation with the def2-TZVP/JK auxiliary basis set were chosen,[36] starting from orbitals and geometries obtained by DFT calculations. The metal d-based orbitals were manually identified and rotated into the active space.

Molecules and orbitals were analyzed, and molecule pictures were created with Chemcraft.[37] Force constants were calculated with *orca_vib*, and orbital cube files were generated with *orca_plot*.[22,23]

Model Systems. One major limitation of the Oxo Wall concept is its applicability to six-coordinate tetragonal complexes only. In order to ensure an approximate six-coordinate tetragonal geometry for the calculated model complexes and to prevent undesired ligand dissociation, a highly tethered ligand system was chosen. The ligand system is based on aromatic and aliphatic amines in the *xy* plane of the metal center. These were chosen in order to minimize the interaction with the d orbitals of (approximate) t_{2g} symmetry, while retaining a rigid coordination geometry. Pyridyl ligands are known to act as π-acceptor ligands. However, for the highly oxidized systems of the present study, this effect should be negligible, and we have indeed not found any evidence for backbonding of the metal into the pyridyl ligand in the calculations. A carboxylate anchor was used trans to the X ligand (X = F or O). The negative charge of the carboxylate group ensures that it stays bound to the metal, even with a potentially strong trans effect that the ligand X may impose. A second important feature of the chosen ligand is its low propensity to form ligand radical complexes. This is important in order to properly focus on the electronic structure of the metal-X bond. While one could argue that there are practically no limitations regarding the complexity of the ligand, we have made an effort to keep the ligand as simple as possible. By choosing the N-substituted pyridinophane core structure, we ensure the applicability of our model system for future experimental investigations since several synthetic routes for this moiety have already been published.[38−40]

The considered oxidation state of the metal for all fluoro and oxo complexes of the 12 chosen transition metals surrounding the Oxo Wall is IV (cf. Figure 1). This oxidation state was chosen for two reasons: (1) For lower oxidation states the stability of the complexes is not guaranteed. (2) In oxidation state IV, the group 9 elements have 5 d electrons, which would theoretically be sufficient for the stabilization of an oxo ligand, which would conceptually be in violation of the Oxo Wall. However, group 9 oxo complexes with six-coordinate tetragonal geometry have not been observed experimentally, even in higher oxidation states. Therefore, using the oxidation state IV allows us to address this discrepancy between concept and experiment. As a final note, we state that the group 9 and 10 oxo complexes considered here do give stable complexes, albeit only under *in silico* and *in vacuo* conditions.

DOI: 10.1021/acs.inorgchem.9b03474
Inorg. Chem. 2020, 59, 1556−1565

RESULTS

Geometries. The M−X bond lengths of the most stable spin states (ground states) of the calculated complexes are summarized in Table 1. In addition, a N−M−N bond angle is given that refers to the pyridyl moieties on the *y*-axis. This angle is a reasonable measure for the deviation from six-coordinate tetragonal geometry, which is especially important for group 9 and 10 complexes (those beyond the Oxo Wall). The full spin-state analysis as well as the ground-state complex geometry coordinates are given in the Supporting Information.

Table 1. Group and Formal Metal d Electron Count, M−X Bond Lengths, (py)N−M−N(py) Bond Angles (along *y* Axis), and Ground-State Spin Multiplicities (2*S* + 1) for All Calculated M−X Complexes

		X = F			X = O		
group	metal center	M−F bond length [Å]	N−M−N angle [deg]	spin mult.	M−O bond length [Å]	N−M−N angle [deg]	spin mult.
7 (d^3)	Mn	1.769	176.1	4	1.655	166.5	4
	Tc	1.879	166.5	4	1.687	151.1	2
	Re	1.904	164.9	4	1.707	148.5	2
8 (d^4)	Fe	1.741	177.1	3	1.629	168.1	3
	Ru	1.848	167.5	3	1.753	162.1	3
	Os	1.874	166.0	3	1.782	159.7	3
9 (d^5)	Co	1.773	179.5	2	1.790	176.1	2
	Rh	1.905	176.7	2	1.892	171.6	2
	Ir	1.900	171.7	2	1.887	171.4	2
10 (d^6)	Ni	1.789	179.6	1	1.792	175.3	3
	Pd	1.923	179.3	1	1.899	177.8	1
	Pt	1.946	179.5	1	1.921	178.9	1

Force Constants. While bond lengths are known to be a reasonable indicator of bond strength, other geometric parameters like bond angles influence the M−X bond length and prevent a clear-cut correlation between the bond length and bond strength. Therefore, the M−X force constants were analyzed, because they provide a more direct and reliable measure of the bond strength (Figure 4). The force constants of the M−F bonds only show minor variations (2.7−4.2 mdyn/Å). The force constants of the M−O bonds, however, reveal a greater variance (1.9−7.9 mdyn/Å) with a clear and consistent discontinuity between group 8 and 9 elements, exactly at the location of the Oxo Wall.

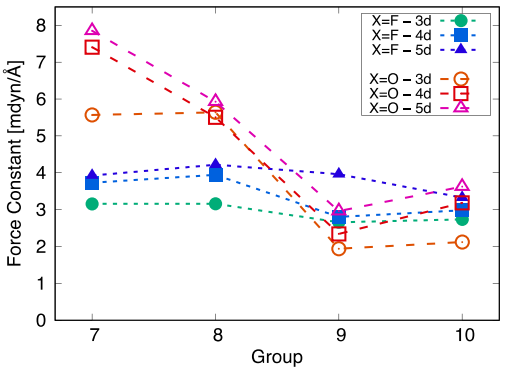

Figure 4. Force constants of M−X bonds for X = F and X = O. Exact values are given in the Supporting Information.

The force constants in Figure 4 indicate that the oxo ligand tends to form bonds of higher order for group 7 and 8 complexes whereas the fluoro ligand does not—which is in agreement with Lewis structure considerations and experimental observations,[41] and also with theoretical studies of transition metal fluoro complexes.[42,43] In order to understand the origin of this behavior, as well as the weak bonding of the oxo ligand with group 9 elements, the orbital structure of the complexes was analyzed.

Electronic Structure. *Orbital Pattern.* As a representative picture for all complexes, the 3d quasi-restricted orbitals (QRO) of the Mn−F and Mn−O complexes are presented in Figure 5.

As expected, the d-orbitals in the six-coordinate tetragonal complexes are separated into a low-lying t_{2g}-like set and a higher-lying e_g-like set, in accordance with approximate O_h symmetry. The lowest orbital is the nonbonding d_{xy} orbital. The large separation of the t_{2g} and e_g sets explains why most of the d^3 systems (Mn, Tc, Re) as exemplified in Figure 5 have a $S = 3/2$ ground state, why the d^4 systems (Fe, Ru, Os) are $S = 1$, why the d^5 systems (Co, Rh, Ir) are $S = 1/2$, and why most of the d^6 systems (Ni, Pd, Pt) are $S = 0$ (cf. Table 1). There are two exceptions to these general observations. The first is the low-spin configuration for the d^3 complexes Tc−O and Re−O ($S = 1/2$), which upon inspection of the orbital structure of these complexes is a consequence of the increased energy difference between the lowest nonbonding t_{2g} orbital and the two antibonding π^* type t_{2g} orbitals (intra-t_{2g} splitting). For Tc−O and Re−O, this energy gap is large enough that the double population of the lowest orbital is energetically favorable, leaving the highest t_{2g} orbital empty. The second is the Ni−O complex (d^6), which features a triplet ground state with a singly occupied orbital from the e_g set (*vide supra*). The localization and stabilization of the lowest e_g orbital indicates that the weakest ligand field is induced by the aliphatic nitrogen atoms of the ligand. We will come back to this subject later in the framework of the angular overlap model.

A thorough comparative analysis of the composition of the QROs of the fluoro and oxo complexes led to two interesting observations. Most noticeably, the oxo complexes of the group 9 elements as well as the Ni−O complex hold a singly occupied p orbital rather localized on the oxo ligand than on the metal (cf. Figure 6), even though this orbital formally constitutes the energetically highest orbital of the t_{2g} set. The presence of a singly occupied p(O) orbital implies a formal metal oxidation state of III instead of the expected oxidation state of IV, rendering the oxo ligand as an oxyl radical ligand. While one would intuitively expect the singly occupied orbital of the group 9 elements to be a metal d orbital, the large p(O) character of the e_g orbital indicates that the order of the d(M) and p(O) orbitals has changed and that from group 9 on, the p(O) orbitals are the highest (singly) occupied QROs. The formal oxidation state of III implies a d electron count of 6 instead of 5 for the group 9 elements, all located in the t_{2g} orbitals set. In other words, one could say that the p(O) orbitals can no longer sufficiently interact with the d(M) orbitals, resulting in a formal bond order of 1. Together with the reduced oxidation state of the metal and the transformation of the oxo ligand into a weaker bonding oxyl radical ligand, the significant and uniform reduction of the force constant for the group 9 M−O complexes (cf. Figure 4) is a logical consequence.

DOI: 10.1021/acs.inorgchem.9b03474
Inorg. Chem. 2020, 59, 1556−1565

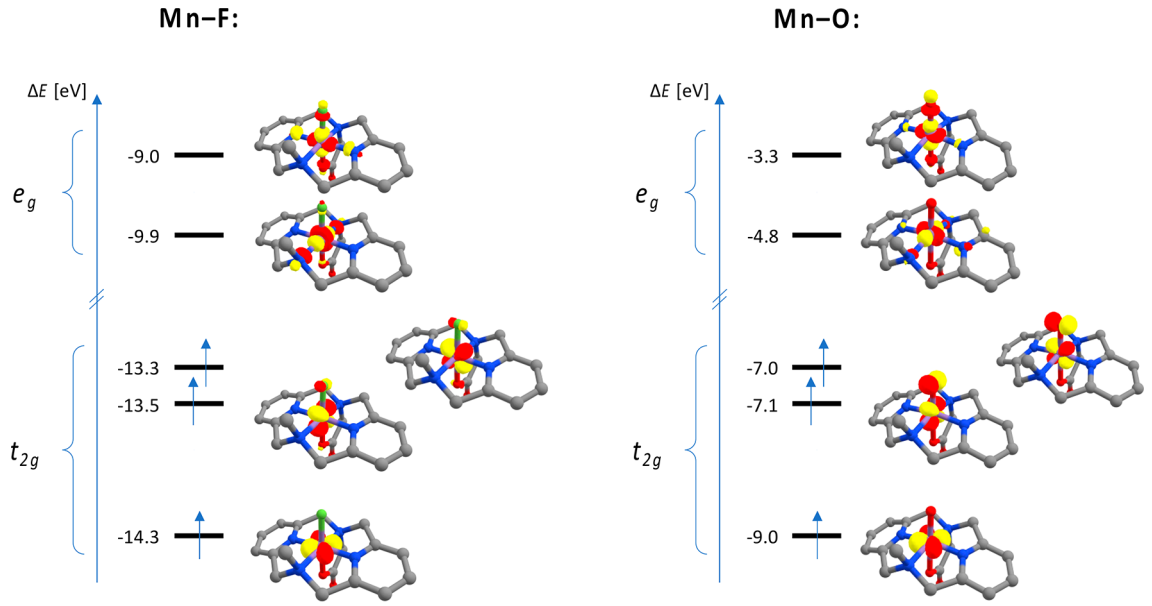

Figure 5. Representative orbital diagram for the d type QROs with energies, orbital pictures, and grouping terms ("t_{2g}", "e_g"; note that these are descriptive terms only and do not state actual degeneracy) of Mn−F (left) and Mn−O (right) complexes. Hydrogens are omitted for clarity (PBE0-D3/def2-TZVP, iso = 0.1).

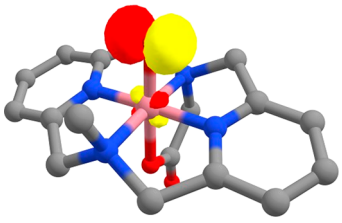

Figure 6. Singly occupied QRO of the Co−O complex. Hydrogens are omitted for clarity (PBE0-D3/def2-TZVP, iso = 0.1).

The latter analysis also holds true for the Ni−O complex, which is the only group 10 complex with a triplet ground state. The QROs reveal a singly occupied p(O) orbital as well as a singly occupied orbital that can be described as a d_{x^2}(Ni) orbital. These two orthogonal orbitals are close enough in energy to give rise to a high-spin configuration, resulting in a Ni(III) center with an oxyl radical ligand. Figure 7 gives a comprehensive overview of the electronic ground states of the calculated group 9 and 10 oxo and fluoro complexes. The increased d electron count in the Ni−O complex results in a bond length extension of all nickel−ligand bonds, most noticeably for the aliphatic amines, which are the weakest ligands. The force constant of the Ni−O bond, of a value in between those of the Co−O and the Rh−O bonds, is also in agreement with this interpretation (cf. Figure 4).

The elevated radical character on oxygen in the formal Co^{III}−O, Rh^{III}−O, and Ir^{III}−O complexes directly to the right side of the Oxo Wall (Figure 1) and that of the Ni^{III}−O complex explains why it has so far proven elusive to synthesize

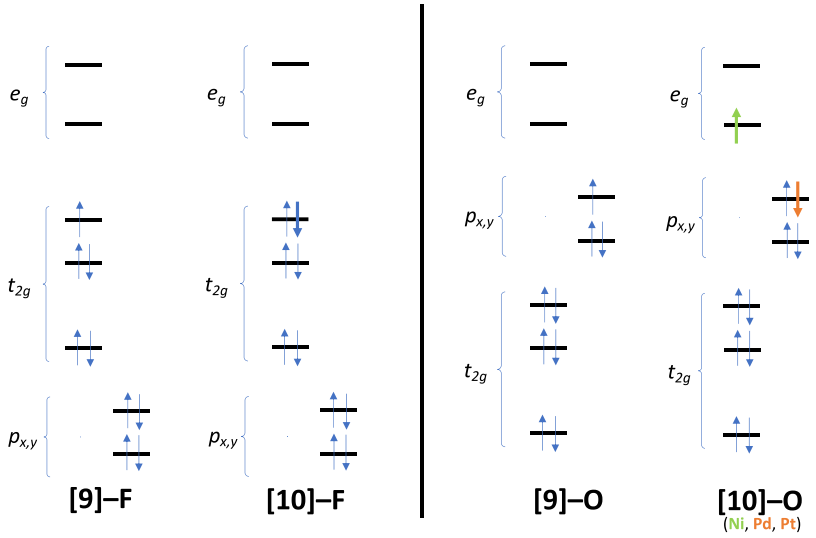

Figure 7. Qualitative depiction of the group 9 ([9]) and 10 ([10]) complexes' electronic ground states. The difference for the group 10 oxo complexes is shown through color: The green electron in the e_g orbital depicts the high-spin ground state of the Ni−O complex, while the orange electron in the p orbital depicts the low-spin ground state of the Pd−O and Pt−O complexes.

DOI: 10.1021/acs.inorgchem.9b03474
Inorg. Chem. 2020, 59, 1556−1565

such compounds. Even though the basic theoretical explanation of the Oxo Wall concept in principle allows for the existence of six-coordinate tetragonal group 9 oxo complexes with an oxidation state of IV and higher (and consequently the existence of tetragonal group 10 oxo complexes with an oxidation state of V and higher, and so on), the answer lies in the orbital order and the reactivity of the resulting oxyl species. Interestingly, throughout the analysis this behavior was never observed in any fluoro complex, which is consistent with the successful synthesis of six-coordinate tetragonal metal fluoro complexes with elements beyond group 8.[41]

The second observation also explains the tendency of the oxo ligand to form multiple bonds, while the fluoro ligand does not. Linear combination of a p(X) and d(M) atomic orbital results in a set of orbitals where the first can be denoted "p", after its major contributor, or "π", due to its bonding character, and the second can be denoted "d" or "π*". For the sake of the argument, the threshold for an atom-centered orbital denotation was set to 0.75. Orbital populations at X or M above this value were denoted p or d orbitals respectively, orbital populations below this value at X or M were denoted π- or π*-orbitals, dependent on their symmetry. It is clear that setting such a threshold to change nomenclature is somewhat arbitrary. However, no major conclusions are drawn that depend on the precise value of this threshold. Given that orbitals and populations are not physical observables, a discussion like the one we provide here is of a qualitative, chemical interpretation-oriented nature in the first place.

Choosing Mn as a specific example, Figure 8 compares the shape of one of the two sets of p/π- and d/π*-type QROs

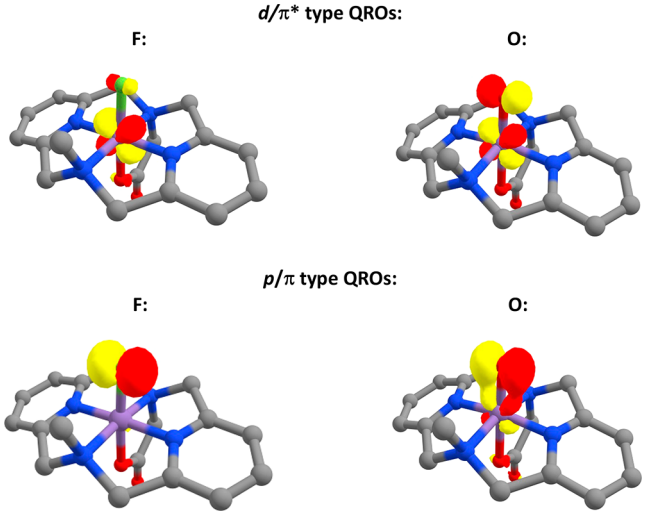

Figure 8. d_{yz}/π_y* and p_y/π_y QROs of Mn−X complexes for X = F (left) and X = O (right). Hydrogens are omitted for clarity (PBE0-D3/def2-TZVP, iso = 0.1).

between the Mn−F and Mn−O complexes. It becomes obvious that the AO-like p- and d-types of QROs dominate for the Mn−F complex, while the bonding/antibonding π- and π*-types of QROs dominate the Mn−O complex. This observation explains the tendency of the M−O complexes to form bonds of higher order, especially in those cases where the antibonding π*-type orbitals are not filled, while the M−F complexes do not have that propensity.

In order to quantify the p/π- and d/π*-type QRO shapes from Figure 8, Table 2 summarizes the mean Loewdin orbital

Table 2. Mean Loewdin Orbital Populations of p/π and d/π* QROs of Mn−X Complexes

Loewdin orb. population	X = F	p/π X = O	X = F	d/π* X = O
d(Mn)	0.07	0.23	0.85	0.65
p(X)	0.90	0.52	0.05	0.28

populations at Mn and X of the Mn−X complexes for X = F and X = O. On the basis of the specification above, the considered orbitals have been denoted p and d for X = F and π and π* for X = O. The enhanced π-bonding of the oxo ligand can be attributed to a higher covalency of the Mn−O bond compared to that of the Mn−F bond, which is also reflected in the Mn−X force constants (cf. Figure 4).

AILFT Analysis and AOM Parameters. In order to further quantify the ability of the oxo ligand over the fluoro ligand to form π-bonds with the coordinated metal, an AILFT analysis was performed. The AILFT module in ORCA deduces the d-orbital energies of a metal through the AILFT reconstruction of a CASSCF calculation that leads to a ligand field matrix $\mathbf{V}^{LFT}$ that is subsequently diagonalized to yield ligand field orbital energies.[20,21] From the 15 independent one-electron parameters of the AILFT Hamiltonian ($\mathbf{V}^{LFT}$), one can also extract ligand and metal specific M−L interaction parameters following the angular overlap model (AOM),[44−46] which can be interpreted as geometry-dependent splitting parameters for individual ligands. Details on the method used to calculate the AOM parameters as well as the full list of calculated parameters can be found in the Supporting Information.

Figure 9 shows a comparison of the d orbital splitting for the Mn−F and Mn−O complexes. While the individual values vary

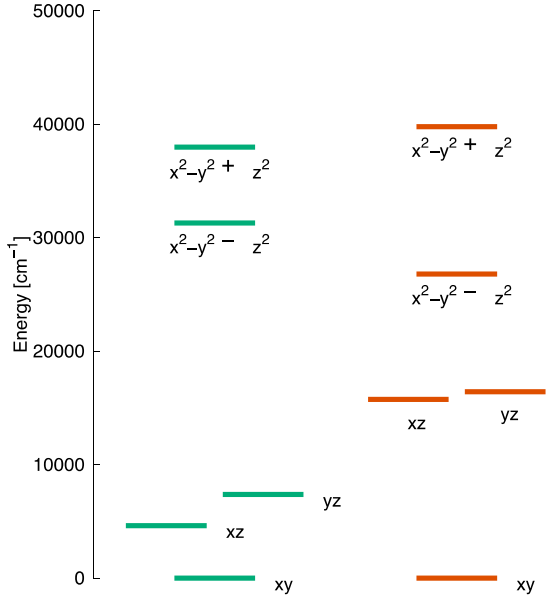

Figure 9. Splitting pattern (d orbital) for Mn−X model complex with X = F (left) and X = O (right).

through the series of evaluated metals, the qualitative picture from Figure 8 is consistent for the other metal complexes as well (for further details see the Supporting Information).

The most striking feature of Figure 9 is certainly the strongly reduced splitting in the t_{2g} set of orbitals for the fluoro ligand. Since the intra-t_{2g} splitting reflects π-bonding, this quantifies the statement that the fluoro ligand is far less involved in π-

DOI: 10.1021/acs.inorgchem.9b03474
Inorg. Chem. 2020, 59, 1556−1565

bonding than the oxo ligand. From the orbital splitting pattern in Figure 9, one can also see that the d_{xz} and d_{yz} orbitals are not completely degenerate. This is due to the influence of the carboxylate ligand, which imposes anisotropic π-donation. This anisotropic ligation results in an anisotropic trans effect on the X ligand, which while normally of isotropic nature, in turn also becomes anisotropic. Hence, the resulting AOM parameters are not only divided into e_σ and e_π, but the e_π parameter is again divided into $e_{\pi s}$ and $e_{\pi c}$. Because the subscripts "s" and "c" stand for "sine" and "cosine" and in spherical coordinate systems the azimuthal angle φ is defined to start at the x axis, $e_{\pi s}$ is defined as the parameter describing the influence of the X ligand on the d_{yz} orbital, and $e_{\pi c}$ is defined as the parameter describing the influence of the X ligand on the d_{xz} orbital. Hence, $e_{\pi s}$ is the parameter influenced more by the anisotropic trans effect of the carboxylate ligand, while $e_{\pi c}$ is expected to pose negligible influences.

Table 3 summarizes the three mean AOM parameters for the fluoro and oxo ligand as well as the individual differences

Table 3. Mean AOM Parameters with Standard Deviations (SD)

X	e_σ [cm^{-1}]	(SD)	$e_{\pi s}$ [cm^{-1}]	(SD)	$e_{\pi c}$ [cm^{-1}]	(SD)
F	15600	(3000)	2000	(1300)	3700	(1300)
O	20400	(6900)	10400	(2700)	13900	(1900)
diff.	4800		8400		10200	

between those two ligands. It is obvious from these values that the σ-donor propensity fluoride is only slightly lower than that of oxygen. However, the key difference is the oxo ligand's ability to form π-bonds, while the fluoride ligand is essentially non-π-bonding despite having occupied orbitals of the correct symmetry. This is reflected by the π-interaction parameters that are 4−5 times lower for the fluoro than for the oxo ligand (see also Figure 8).

Relative Orbital Energies. Because overlap (i.e., spatial interactions) between p(X) and d(M) orbitals is expected to be rather similar for X = F and O, the difference between F and O in the interaction between the p(X) and d(M) orbitals can presumably be attributed to their energy differences. In order to quantify the orbital energy differences, the following model was deployed. The QRO that most resembled a p(X) orbital was located, and the energy relative to the rather nonbonding d_{xy} QRO was determined and cached. The latter orbital energy, $\epsilon_{d_{xy}}$, is assumed to be independent from electronic interactions of the X ligand. For a given metal complex M, the relative energy difference between the p(F) and the p(O) orbital of the proper X ligand was subsequently estimated from the cached values:

$$\Delta E_M = (\Delta p_O - \Delta p_F)_M = (\epsilon_p - \epsilon_{d_{xy}})_{M-O} - (\epsilon_p - \epsilon_{d_{xy}})_{M-F} \quad (1)$$

The thus obtained p(X) orbital energy differences are plotted in Figure 10. The value of ΔE states in good approximation for each metal how much deeper the p(F) orbital lies relative to the p(O) orbital. Relative to the nonbonding d_{xy}(M) orbital, most of the p(F) orbitals are found between 2 and 3 eV lower than their p(O) counterparts, with the difference rising up to 3.6 eV. Furthermore, a clear slope can be identified to the right side of the location of the Oxo Wall. This slope can be

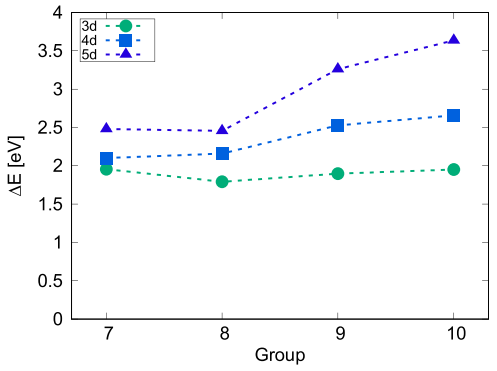

Figure 10. Energy difference of p(F) and p(O) according to eq 1.

attributed to the decreasing interaction between the p(O) and the d(M) orbitals going from group 7 to group 10 oxo complexes as already described above.

Natural Population Analysis and NMR Parameters. We address the final open question, the theoretical explanation of the instability of the closed shell group 10 oxo compounds (i.e. the Pd−O and the Pt−O complexes) through a natural population analysis (NPA), especially for the p(X) orbitals. Even without the significant radical character of the X ligands of the closed shell group 10 M−X complexes, the NPA reveals an electron deficiency especially on the oxo ligands, which after MO theory can be described as a singly bound ligand with a one-electron-equivalent formal charge remaining on the ligand. The NPA impressively shows that the p_z(O) orbitals for the Pd−O and Pt−O complexes, which are the orbitals mostly involved in the M−O σ-bond, lack nearly a full net electron. This makes the oxo ligand a strong electrophile and oxidant, likely resulting in complexes too reactive to be experimentally observed. Overall, the generally decreased population of the p_z(O) orbitals compared to the p_z(F) orbitals is also a strong argument for the rather covalent character of the M−O bond and the more ionic character of the M−F bond, in agreement with the afore-described findings of the orbital analysis. While the latter focused on the M−X π bonds, the NPA findings complement the analysis by addressing the covalency of the σ-bonds between the metals and the X ligands.

In order to correlate the results of the NPA to measurable quantities, NMR shifts of the closed shell complexes were calculated. Table 4 gives the calculated values of the NPA and

Table 4. Calculated NPA and NMR Parameters of Group 10 M−X Complexes

	Ni−X		Pd−X		Pt−X	
	X = F	X = O	X = F	X = O	X = F	X = O
NPA: Σp(X)[a]	5.640	4.601	5.654	5.019	5.653	5.106
NPA: p_z(X)	1.663	1.559[b]	1.672	1.085	1.670	1.196
NMR: δ(X) [ppm]	−288.7		−189.0	1251.9	−208.8	632.7

[a]Sum of NPA values of p_x(X), p_y(X), and p_z(X). [b]p_y(O) = 1.061.

of the NMR shifts. Comparing the overall p(X) population (row 1) with the NMR shifts, it becomes obvious that the lack of electron density on the X ligand correlates smoothly with the NMR shifts. This correlation can be explained through the deshielding effect on the nuclei by a less populated p(X) shell.

Comparison of the calculated NMR shifts in Table 4 with experimental data is difficult, because reported NMR shifts are

DOI: 10.1021/acs.inorgchem.9b03474
Inorg. Chem. 2020, 59, 1556−1565

found on an extremely wide range for both nuclei. ^{19}F NMR shifts of palladium fluoro complexes are typically found in the range of −274 to −323 ppm.[19,47−50] The example of a palladium difluoride with ^{19}F NMR shifts of −169 and −278 ppm, however, not only shows that the range of shifts is even greater but also shows that they can also drastically differ within the same complex.[51] For platinum fluoro complexes, the range of ^{19}F NMR shifts is even greater and typically spans from −107 to −456 ppm.[52,53] For nickel fluorides, ^{19}F NMR shifts are typically reported between −251 and −423 ppm.[54,55] In contrast to the fluoro complexes, the reported oxo complexes are purely hypothetical. Additionally, to the best of our knowledge, ^{17}O NMR shifts of group 10 oxo metal complexes are not reported. ^{17}O NMR shifts of other transition metal oxo complexes are reported between 775 and 1247 ppm.[56] For comparison, the proposed[13,57,58] and later retracted[14] late transition metal oxo complexes by Hill et al. had ^{17}O NMR shifts at 570, 590, and 605 ppm assigned to palladium and gold oxo complexes and a shift at 330 ppm assigned to a palladium hydroxo complex. All of them were later attributed to the polyoxotungstate ligands. While the calculated values for the fluoro complexes are in decent agreement with measured values of comparable complexes, the calculated values of the hypothetical oxo complexes are beyond the reported range, which is in agreement with the expected instability of the proposed structures.

DISCUSSION

In general,[59] the linear combination of two heteronuclear atomic orbitals A and B form a bonding/antibonding combination n/n^*, which can be approximately described as

$$n = N_1(\mathrm{A} + \alpha\cdot\mathrm{B}) \tag{2}$$

$$n^* = N_2(\mathrm{B} - \alpha\cdot\mathrm{A}) \tag{3}$$

with N_i being the normalization constants and α being an orbital weighing factor derived from first-order perturbation theory[60,61] and applied to extended Hückel theory:[62,63]

$$\alpha \propto \frac{\beta}{\epsilon_\mathrm{A} - \epsilon_\mathrm{B}} \tag{4}$$

with the resonance integral β and the atomic orbital energies ϵ_i. The Principle of Maximum Overlap[64−66] simplifies the correlation between the resonance integral β and the (spatial) overlap integral S_{AB} as

$$\beta \propto S_{AB} \tag{5}$$

The expected energy shift of the orbitals $\delta \approx \epsilon_n - \epsilon_\mathrm{A} \approx \epsilon_\mathrm{B} - \epsilon_{n^*}$ can be approximated as follows:

$$\delta \approx \frac{\beta^2}{\epsilon_\mathrm{A} - \epsilon_\mathrm{B}} \tag{6}$$

From eqs 2−5, it is obvious that there are two major factors influencing the mixing of orbitals A and B: the orbitals mix more for larger spatial overlap as well as for a smaller difference between the atomic orbital energies. This means that for $S_{AB} \to 0$ and for $\epsilon_\mathrm{A} \ll \epsilon_\mathrm{B}$ the values of n and n^* will resemble A and B, respectively (i.e., $\alpha = 0$), rather than a linear combination of A and B, also depicted by the vanishing energy shift of the orbitals as shown in eq 6. While this model is too simplistic to actually derive meaningful values from it, it paints a qualitative picture that is certainly sufficient to set the values calculated in the "Results" section into context.

In the first approximation (cf. eq 5), the resonance integral β can be treated as proportional to the spatial overlap of orbitals A and B. Due to the reduced charge of the fluoro ligand compared to the oxo ligand, the 1p orbitals of the fluoro ligand are expected to have a smaller radial expectation value than that of the oxo ligand and consequently also a reduced overlap. Indeed, the radial expectation values for the 1p orbitals were calculated as 1.21 and 1.58 Å for fluoride and oxide, respectively. The same trends that are obvious in Figure 4 can be expected to hold for β as well. This result is also consistent with the larger force constants calculated for the group 7 and 8 oxo complexes (cf. Table 1).

The calculated AOM parameters (cf. Table 3) can be interpreted as δ values (cf. eq 6) for different orbital interactions: $e_{\pi c}$ and $e_{\pi s}$ approximately equal δ for the interaction between the d_{xz}(M) and p_x(X), as well as d_{yz}(M) and p_y(X) orbitals, respectively. In addition, the ΔE values from Figure 10 (derived from eq 1) exactly quantify the difference between X = F and X = O as $\epsilon_{p(X)} - \epsilon_{d(M)}$. Hence, it can be directly deduced from these ΔE values that assuming a comparable β the δ values for X = F are expected to be smaller than those for X = O (because the denominator in eq 6 is bigger for X = F), which agrees with the AOM parameters.

Comparing eqs 4 and 6, one would expect a trend for α similar to that for δ. Indeed, comparing the mean Loewdin orbital populations from Table 2 (depicted in Figure 8), one can see that the orbital mixing between the p(X) and d(M) orbitals is much smaller for X = F than for X = O. This is the direct consequence of a smaller α value in eq 2, resulting from the larger orbital energy difference in eq 4 for X = F than for X = O.

The p(F) orbital has a lower energy than the p(O) orbital due to the higher effective nuclear charge experienced by the 2p electrons for fluorine since the increased nuclear charge of the fluorine nucleus is incompletely shielded by the other electrons. The difference of the p orbital energy between F and O has implications for the analyzed fluoro and oxo complexes: While the p(F) orbitals simply remain inaccessible for multiple bonding, the p(O) orbitals are so exposed that if not stabilized through d(M) interactions then a singly bound oxo ligand would be extremely reactive and hence unstable. In some instances met in our calculations, the oxidation potential of the metal center is already high enough to draw an electron out of a p(O) orbital, resulting in an oxyl radical complex. The NPA of the p_z(O) orbitals in Table 4 reveals that the oxo ligands in the hypothetical Pd−O and Pt−O complexes are so electron-deficient that they will likely react with even extremely weak electron donors by oxidation or oxygenation. Potential stabilization of those complexes by more electron-donating ligands to shift the electrons more toward the oxo ligand will instead result in increased basicity, eventually leading to already well-known and studied hydroxyl complexes (and probably deprotonated solvent).

Synthetically, we can think of two ways in which these results can be utilized. First, the energetic mingling of the d manifold and the p(O) orbitals observed for the group 9 and 10 oxo complexes leads to the formation of oxyl radical complexes in some cases. Tweaking the electronic properties of the ligand (e.g., by adding electron-withdrawing substituents like F, CF_3, or NO_2 to the pyridyl moieties) can potentially lead to an energetic stabilization of the d manifold, possibly

DOI: 10.1021/acs.inorgchem.9b03474
Inorg. Chem. 2020, 59, 1556−1565

strong enough to form oxyl radical complexes with group 8 or even group 7 metals. Further fine-tuning could eventually lead to "designer complexes" with oxyl character, potentially exhibiting unprecedented (catalytic) properties. Second, although chemically extremely challenging, we consider pushing the limits to a point where a late transition metal d manifold can be stabilized by extremely electron-withdrawing ligands to an extent where chemically meaningful interactions with the p(F) orbitals are possible, practically resulting in M−F multiple bonding. However, to date this has admittedly never been observed experimentally. The targeted search for such unusual compounds is, however, at the heart of chemical curiosity.

CONCLUSIONS

Through an extensive computational analysis of the geometric and electronic structure of a series of model complexes around the Oxo Wall, we solidified the theoretical foundation of the Oxo Wall concept. We have shown that the p orbitals of oxo ligands are energetically more readily accessible than the p orbitals of fluoro ligands by more than 2 eV. This leaves the fluoro ligand practically inaccessible for multiple bonding and the oxo ligand too reactive for formation of stable complexes with a singly bound oxo species. Hence, we conclude that there is no theoretically justifiable or practically meaningful concept of a Fluoro Wall. While the present analysis mostly focused on π-bonding, AOM and NPA analyses suggest that differences in σ-bonding also play a crucial role. According to our analysis, the M−F σ-bond seems to possess a rather ionic character, while the M−O σ-bond is of a more covalent nature, which is likely the source of the high electrophilicity and oxidative power of the oxo-complexes beyond the Oxo Wall, resulting in their practical instability. However, further research is required to evaluate the subtle differences in detail.

ASSOCIATED CONTENT

Supporting Information

The Supporting Information is available free of charge at https://pubs.acs.org/doi/10.1021/acs.inorgchem.9b03474.

Complete spin state analysis, Cartesian coordinates of all geometry optimized model structures, force constants, and full AILFT analysis, including AOM parameters- (PDF)

AUTHOR INFORMATION

Corresponding Authors

*E-mail: maurice.van-gastel@kofo.mpg.de (M.v.G.).
*E-mail: frank.neese@kofo.mpg.de (F.N.).

ORCID

Maurice van Gastel: 0000-0002-1547-6365
Frank Neese: 0000-0003-4691-0547

Notes

The authors declare no competing financial interest.

ACKNOWLEDGMENTS

Support by the Max Planck Society is gratefully acknowledged. J.D.R. thanks the Fonds der Chemischen Industrie for funding and Mihail Atanasov for insightful discussions regarding ligand-field theory.

REFERENCES

(1) Winkler, J. R.; Gray, H. B. In *Molecular Electronic Structures of Transition Metal Complexes I*; Mingos, D. M. P., Day, P., Dahl, J. P., Eds.; Springer Berlin Heidelberg: Berlin, Germany, 2011; Chapter 55, Vol. *142*, pp 17−28.
(2) Meunier, B.; de Visser, S. P.; Shaik, S. Mechanism of oxidation reactions catalyzed by cytochrome p450 enzymes. *Chem. Rev.* **2004**, *104* (9), 3947−80.
(3) Gray, H. B.; Winkler, J. R. Living with Oxygen. *Acc. Chem. Res.* **2018**, *51* (8), 1850−1857.
(4) Ballhausen, C. J.; Gray, H. B. The Electronic Structure of the Vanadyl Ion. *Inorg. Chem.* **1962**, *1* (1), 111−122.
(5) Gray, H. B.; Hare, C. R. The Electronic Structures and Spectra of Chromyl and Molybdenyl Ions. *Inorg. Chem.* **1962**, *1* (2), 363−368.
(6) Frenking, G.; Krapp, A. Unicorns in the world of chemical bonding models. *J. Comput. Chem.* **2007**, *28* (1), 15−24.
(7) Sunil, K. K.; Harrison, J. F.; Rogers, M. T. An SCF−MS−Xα study of a series of d1 transition metal oxohalo complexes. *J. Chem. Phys.* **1982**, *76* (6), 3087−3097.
(8) Garner, C. D.; Kendrick, J.; Lambert, P.; Mabbs, F. E.; Hillier, I. H. Single-crystal electronic spectrum of tetraphenylarsonium oxotetrachlorochromate(V), [C6H5)4As][CrOC14], and an ab initio calculation of the bonding and excited states of oxotetrachlorochromate(V). *Inorg. Chem.* **1976**, *15* (6), 1287−1291.
(9) Azuma, N.; Ozawa, T.; Tsuboyama, S. Spectroscopic studies of a square-pyramidal nitridochromium(V) complex. *J. Chem. Soc., Dalton Trans.* **1994**, No. 18, 2609.
(10) Hay-Motherwell, R. S.; Wilkinson, G.; Hussain-Bates, B.; Hursthouse, M. B. Synthesis and X-ray crystal structure of oxotrimesityliridium(V). *Polyhedron* **1993**, *12* (16), 2009−2012.
(11) Poverenov, E.; Efremenko, I.; Frenkel, A. I.; Ben-David, Y.; Shimon, L. J. W.; Leitus, G.; Konstantinovski, L.; Martin, J. M. L.; Milstein, D. Evidence for a terminal Pt(iv)-oxo complex exhibiting diverse reactivity. *Nature* **2008**, *455* (7216), 1093−1096.
(12) Munz, D. How to tame a palladium terminal oxo. *Chem. Sci.* **2018**, *9* (5), 1155−1167.
(13) Anderson, T. M.; Neiwert, W. A.; Kirk, M. L.; Piccoli, P. M.; Schultz, A. J.; Koetzle, T. F.; Musaev, D. G.; Morokuma, K.; Cao, R.; Hill, C. L. A late-transition metal oxo complex: K7Na9[O = PtIV(H2O)L2], L = [PW9O34]9. *Science* **2004**, *306* (5704), 2074−7.
(14) O'Halloran, K. P.; Zhao, C.; Ando, N. S.; Schultz, A. J.; Koetzle, T. F.; Piccoli, P. M.; Hedman, B.; Hodgson, K. O.; Bobyr, E.; Kirk, M. L.; Knottenbelt, S.; Depperman, E. C.; Stein, B.; Anderson, T. M.; Cao, R.; Geletii, Y. V.; Hardcastle, K. I.; Musaev, D. G.; Neiwert, W. A.; Fang, X.; Morokuma, K.; Wu, S.; Kogerler, P.; Hill, C. L. Revisiting the polyoxometalate-based late-transition-metal-oxo complexes: the "oxo wall" stands. *Inorg. Chem.* **2012**, *51* (13), 7025−31.
(15) Berry, J. F. Terminal Nitrido and Imido Complexes of the Late Transition Metals. *Comments Inorg. Chem.* **2009**, *30* (1−2), 28−66.
(16) Laskowski, C. A.; Miller, A. J.; Hillhouse, G. L.; Cundari, T. R. A two-coordinate nickel imido complex that effects C-H amination. *J. Am. Chem. Soc.* **2011**, *133* (4), 771−3.
(17) Drews, T.; Supel, J.; Hagenbach, A.; Seppelt, K. Solid state molecular structures of transition metal hexafluorides. *Inorg. Chem.* **2006**, *45* (9), 3782−8.
(18) Lee, E.; Kamlet, A. S.; Powers, D. C.; Neumann, C. N.; Boursalian, G. B.; Furuya, T.; Choi, D. C.; Hooker, J. M.; Ritter, T. A fluoride-derived electrophilic late-stage fluorination reagent for PET imaging. *Science* **2011**, *334* (6056), 639−42.
(19) Yamamoto, K.; Li, J.; Garber, J. A. O.; Rolfes, J. D.; Boursalian, G. B.; Borghs, J. C.; Genicot, C.; Jacq, J.; van Gastel, M.; Neese, F.; Ritter, T. Palladium-catalysed electrophilic aromatic C-H fluorination. *Nature* **2018**, *554* (7693), 511−514.
(20) Atanasov, M.; Ganyushin, D.; Sivalingam, K.; Neese, F. In *Molecular Electronic Structures of Transition Metal Complexes II*; Mingos, D. M. P., Day, P., Dahl, J. P., Eds.; Springer Berlin Heidelberg: Berlin, Germany, 2012; Vol. *143*, pp 149−220.
(21) Atanasov, M.; Zadrozny, J. M.; Long, J. R.; Neese, F. A theoretical analysis of chemical bonding, vibronic coupling, and

DOI: 10.1021/acs.inorgchem.9b03474
Inorg. Chem. 2020, 59, 1556−1565

magnetic anisotropy in linear iron(ii) complexes with single-molecule magnet behavior. *Chem. Sci.* **2013**, *4* (1), 139−156.
(22) Neese, F. The ORCA program system. *Wiley Interdisciplinary Reviews: Computational Molecular Science* **2012**, *2* (1), 73−78.
(23) Neese, F. Software update: the ORCA program system, version 4.0. *WIREs Comput. Mol. Sci.* **2018**, *8* (1), e1327.
(24) Adamo, C.; Barone, V. Toward reliable density functional methods without adjustable parameters: The PBE0 model. *J. Chem. Phys.* **1999**, *110* (13), 6158−6170.
(25) Weigend, F.; Ahlrichs, R. Balanced basis sets of split valence, triple zeta valence and quadruple zeta valence quality for H to Rn: Design and assessment of accuracy. *Phys. Chem. Chem. Phys.* **2005**, *7* (18), 3297−305.
(26) Grimme, S.; Antony, J.; Ehrlich, S.; Krieg, H. A consistent and accurate ab initio parametrization of density functional dispersion correction (DFT-D) for the 94 elements H-Pu. *J. Chem. Phys.* **2010**, *132* (15), 154104.
(27) Grimme, S.; Ehrlich, S.; Goerigk, L. Effect of the damping function in dispersion corrected density functional theory. *J. Comput. Chem.* **2011**, *32* (7), 1456−65.
(28) Neese, F. An improvement of the resolution of the identity approximation for the formation of the Coulomb matrix. *J. Comput. Chem.* **2003**, *24* (14), 1740−7.
(29) Weigend, F. Accurate Coulomb-fitting basis sets for H to Rn. *Phys. Chem. Chem. Phys.* **2006**, *8* (9), 1057−65.
(30) Neese, F.; Wennmohs, F.; Hansen, A.; Becker, U. Efficient, approximate and parallel Hartree−Fock and hybrid DFT calculations. A 'chain-of-spheres' algorithm for the Hartree−Fock exchange. *Chem. Phys.* **2009**, *356* (1−3), 98−109.
(31) Hanwell, M. D.; Curtis, D. E.; Lonie, D. C.; Vandermeersch, T.; Zurek, E.; Hutchison, G. R. Avogadro: an advanced semantic chemical editor, visualization, and analysis platform. *J. Cheminf.* **2012**, *4* (1), 17.
(32) Neese, F. Importance of direct spin-spin coupling and spin-flip excitations for the zero-field splittings of transition metal complexes: a case study. *J. Am. Chem. Soc.* **2006**, *128* (31), 10213−22.
(33) Roos, B. O.; Taylor, P. R.; Sigbahn, P. E. M. A complete active space SCF method (CASSCF) using a density matrix formulated super-CI approach. *Chem. Phys.* **1980**, *48* (2), 157−173.
(34) Siegbahn, P.; Heiberg, A.; Roos, B.; Levy, B. A Comparison of the Super-CI and the Newton-Raphson Scheme in the Complete Active Space SCF Method. *Phys. Scr.* **1980**, *21* (3−4), 323−327.
(35) Siegbahn, P. E. M.; Almlöf, J.; Heiberg, A.; Roos, B. O. The complete active space SCF (CASSCF) method in a Newton−Raphson formulation with application to the HNO molecule. *J. Chem. Phys.* **1981**, *74* (4), 2384−2396.
(36) Weigend, F. Hartree-Fock exchange fitting basis sets for H to Rn. *J. Comput. Chem.* **2008**, *29* (2), 167−75.
(37) *Chemcraft - Graphical Software for Visualization of Quantum Chemistry Computations*. https://www.chemcraftprog.com.
(38) Alpha, B.; Anklam, E.; Deschenaux, R.; Lehn, J.-M.; Pietraskiewiez, M. Synthesis and Characterisation of the Sodium and Lithium Cryptates of Macrobicyclic Ligands incorporating pyridine, bipyridine, and biisoquinoline units. *Helv. Chim. Acta* **1988**, *71* (5), 1042−1052.
(39) Bottino, F.; Di Grazia, M.; Finocchiaro, P.; Fronczek, F. R.; Mamo, A.; Pappalardo, S. Reaction of tosylamide monosodium salt with bis(halomethyl) compounds: an easy entry to symmetrical N-tosyl aza macrocycles. *J. Org. Chem.* **1988**, *53* (15), 3521−3529.
(40) Wessel, A. J.; Schultz, J. W.; Tang, F.; Duan, H.; Mirica, L. M. Improved synthesis of symmetrically & asymmetrically N-substituted pyridinophane derivatives. *Org. Biomol. Chem.* **2017**, *15* (46), 9923−9931.
(41) Winfield, J. M. Transition metal fluorides. *J. Fluorine Chem.* **1986**, *33* (1−4), 159−178.
(42) Abu-Hasanayn, F.; Goldman, A. S.; Krogh-Jespersen, K. Ab Initio Molecular Orbital Study of Substituent Effects in Vaska Type Complexes (trans-IrL2(CO)X): Electron Affinities, Ionization Potentials, Carbonyl Stretch Frequencies and the Thermodynamics of H2 Dissociative Addition. *Inorg. Chem.* **1994**, *33* (22), 5122−5130.
(43) Laitar, D. S.; Müller, P.; Gray, T. G.; Sadighi, J. P. A Carbene-Stabilized Gold(I) Fluoride: Synthesis and Theory. *Organometallics* **2005**, *24* (19), 4503−4505.
(44) Figgis, B. N.; Hitchman, M. A. *Ligand Field Theory and Its Applications*; John Wiley & Sons, Ltd.: New York, 2000.
(45) Jørgensen, C. K.; Pappalardo, R.; Schmidtke, H. H. Do the "Ligand Field" Parameters in Lanthanides Represent Weak Covalent Bonding? *J. Chem. Phys.* **1963**, *39* (6), 1422−1430.
(46) Schäffer, C. E.; Jørgensen, C. K. The angular overlap model, an attempt to revive the ligand field approaches. *Mol. Phys.* **1965**, *9* (5), 401−412.
(47) Fraser, S. L.; Antipin, M. Y.; Khroustalyov, V. N.; Grushin, V. V. Molecular Fluoro Palladium Complexes. *J. Am. Chem. Soc.* **1997**, *119* (20), 4769−4770.
(48) Marshall, W. J.; Thorn, D. L.; Grushin, V. V. Single-Crystal X-ray and Solution13C NMR Study of Fluoro(p-nitrophenyl)bis-(triphenylphosphine)palladium(II). Are There Effects of Through-Conjugation?†. *Organometallics* **1998**, *17* (24), 5427−5430.
(49) Jasim, N. A.; Perutz, R. N.; Whitwood, A. C.; Braun, T.; Izundu, J.; Neumann, B.; Rothfeld, S.; Stammler, H.-G. Contrasting Reactivity of Fluoropyridines at Palladium and Platinum: C−F Oxidative Addition at Palladium, P−C and C−F Activation at Platinum†. *Organometallics* **2004**, *23* (26), 6140−6149.
(50) Grushin, V. V.; Marshall, W. J. Facile Ar-CF3 bond formation at Pd. Strikingly different outcomes of reductive elimination from [(Ph3P)2Pd(CF3)Ph] and [(Xantphos)Pd(CF3)Ph]. *J. Am. Chem. Soc.* **2006**, *128* (39), 12644−5.
(51) Furuya, T.; Ritter, T. Carbon-fluorine reductive elimination from a high-valent palladium fluoride. *J. Am. Chem. Soc.* **2008**, *130* (31), 10060−1.
(52) Nilsson, P.; Plamper, F.; Wendt, O. F. Synthesis, Structure, and Reactivity of Arylfluoro Platinum(II) Complexes. *Organometallics* **2003**, *22* (25), 5235−5242.
(53) Yahav, A.; Goldberg, I.; Vigalok, A. Difluoro complexes of platinum(II) and -(IV) with monodentate phosphine ligands: an exceptional stability of d6 octahedral organometallic fluorides. *Inorg. Chem.* **2005**, *44* (5), 1547−53.
(54) Matwiyoff, N. A.; Asprey, L. B.; Wageman, W. E.; Reisfeld, M. J.; Fukushima, E. Fluorine-19 nuclear magnetic resonance studies of diamagnetic fluoride complexes of nickel(IV), palladium(IV), and platinum(IV) in anhydrous hydrogen fluoride solutions. *Inorg. Chem.* **1969**, *8* (4), 750−753.
(55) Meucci, E. A.; Ariafard, A.; Canty, A. J.; Kampf, J. W.; Sanford, M. S. Aryl−Fluoride Bond-Forming Reductive Elimination from Nickel(IV) Centers. *J. Am. Chem. Soc.* **2019**, *141* (33), 13261−13267.
(56) Fujii, H.; Kurahashi, T.; Tosha, T.; Yoshimura, T.; Kitagawa, T. 17O NMR study of oxo metalloporphyrin complexes: correlation with electronic structure of M = O moiety. *J. Inorg. Biochem.* **2006**, *100* (4), 533−41.
(57) Anderson, T. M.; Cao, R.; Slonkina, E.; Hedman, B.; Hodgson, K. O.; Hardcastle, K. I.; Neiwert, W. A.; Wu, S.; Kirk, M. L.; Knottenbelt, S.; Depperman, E. C.; Keita, B.; Nadjo, L.; Musaev, D. G.; Morokuma, K.; Hill, C. L. A Palladium-Oxo Complex. Stabilization of This Proposed Catalytic Intermediate by an Encapsulating Polytungstate Ligand. *J. Am. Chem. Soc.* **2005**, *127* (34), 11948−11949.
(58) Cao, R.; Anderson, T. M.; Piccoli, P. M. B.; Schultz, A. J.; Koetzle, T. F.; Geletii, Y. V.; Slonkina, E.; Hedman, B.; Hodgson, K. O.; Hardcastle, K. I.; Fang, X.; Kirk, M. L.; Knottenbelt, S.; Kögerler, P.; Musaev, D. G.; Morokuma, K.; Takahashi, M.; Hill, C. L. Terminal Gold-Oxo Complexes. *J. Am. Chem. Soc.* **2007**, *129* (36), 11118−11133.
(59) Anh, N. T. In *Frontier Orbitals: A Practical Manual*; Wiley & Sons, Ltd.: New York, 2007; pp 5−24.
(60) Pople, J. A. Molecular orbital perturbation theory II. Charge displacement and stabilization in conjugated molecules. *Proc. R. Soc. Lond. A* **1955**, *233* (1193), 233−241.

DOI: 10.1021/acs.inorgchem.9b03474
Inorg. Chem. 2020, 59, 1556−1565

(61) Libit, L.; Hoffmann, R. Detailed orbital theory of substituent effects. Charge transfer, polarization, and the methyl group. *J. Am. Chem. Soc.* **1974**, *96* (5), 1370−1383.
(62) Hückel, E. Zur Quantentheorie der Doppelbindung. *Eur. Phys. J. A* **1930**, *60* (7−8), 423−456.
(63) Hoffmann, R. An Extended Hückel Theory. I. Hydrocarbons. *J. Chem. Phys.* **1963**, *39* (6), 1397−1412.
(64) Pauling, L. The Nature of the Chemical Bond. Application of Results Obtained from the Quantum Mechanics and from a Theory of Paramagnetic Susceptibility to the Structure of Molecules. *J. Am. Chem. Soc.* **1931**, *53* (4), 1367−1400.
(65) Slater, J. C. Directed Valence in Polyatomic Molecules. *Phys. Rev.* **1931**, *37* (5), 481−489.
(66) Mulliken, R. S. Electronic Structures of Polyatomic Molecules and Valence. II. General Considerations. *Phys. Rev.* **1932**, *41* (1), 49−71.

DOI: 10.1021/acs.inorgchem.9b03474
Inorg. Chem. 2020, 59, 1556−1565